Supporting Information for *Acta Phys. -Chim. Sin.* 2017, *33* (9), 1773−1780
doi: 10.3866/PKU.WHXB201705087

孔洞和孪晶界对银纳米线形变行为联合影响的分子动力学模拟

汪秀秀 [1] 赵健伟 [2,*] 余 刚 [1,*]

([1] 湖南大学化学生物传感与计量学国家重点实验室，化学化工学院，长沙 410082；
[2] 嘉兴学院材料与纺织工程学院，浙江 嘉兴 314001)

Combined Effects of the Hole and Twin Boundary on the Deformation of Ag Nanowires: a Molecular Dynamics Simulation Study

WANG Xiu-Xiu[1] ZHAO Jian-Wei[2] YU Gang[1,*]

([1]*State Key Laboratory of Chemo/Biosensing and Chemometrics, College of Chemistry and Chemical Engineering, Hunan University, Changsha 410082, P. R. China*; [2]*College of Material and Textile Engineering, Jiaxing University, Jiaxing 314001, P. R. China*)

[*]Corresponding authors. YU Gang, Email: yuganghnu@163.com; Tel: +86-1897493643.
ZHAO Jian-Wei, Email: zhaojw@nju.edu.cn; Tel: +86-13967321774.

1. In this paper, before stretching, the model is relaxed in 20000 steps. The time step is 2.5638 fs in our simulation. So, the relaxation time is ($20000 \times 2.5638 \times 10^{-3}$) ps =51.276 ps.
2. Classical MD simulations of Ag nanowires subjected to uniaxial tensile deformation are performed with a self-developed code, NanoMD. The reliability of algorithms has been validated by a large amount of theoretical simulations. The well-established embedded-atom method potential by Johnson is chosen to describe the Ag-Ag atomic interactions. Prior to the tensile loading, each system is needed to be relaxed at a constant temperature to reach a metastable equilibrium state, and then uniaxial tension of Ag nanowires is performed in the canonical NVT ensemble by straining the simulation box along <111> axial direction with constant strain rate. The Verlet leapfrog algorithm is used for the integration of motion equations to obtain velocity and trajectories of atoms. Free boundary behaviour of the nanostructures. The time step utilized in the MD simulation is 0.01τ, where $\tau = 2.6 \times 10^{-13}$ s (τ is the parameter between dimensionless MD unit and real physical unit).
3. Fig.(a) in Fig.1 and 2 corresponds to the true yield point. At true yield point, the initial dislocations are all emitted from the surface in specimen I and III (the letter "A" in Fig.1(a) and 2(a)) and it is not affected by the hole, in accordance with the result of the first stage which the hole has no effect on the initial dislocation generated in Fig.5. Fig.(b) and (c) in Fig.1 and 2 correspond to the yield point and the first release point, respectively. It explains the phenomenon of the speed of the number of HCP atoms increases first increases and then decreases with the increase of the hole radius from microstructure. Compared with specimen IV, the main hole of specimen II, III is as dislocation sources generate new dislocations. While the main role of the hole of specimen IV is blocks the dislocation slips, and the dislocation generated rate is lower than specimen I, II, III corresponding to Fig.6. Fig.(c), a large number of dislocations are generated and partial dislocations are absorbed by twin boundary or the front dislocation. In Fig.8(c), the hole in twin boundary has two roles, one is generates new dislocations as dislocation

sources, and the other is blocks the dislocation slip. Fig.(d) corresponds to the strain is 0.1, where the number of HCP atoms appears fluctuation. In Figure1(d) and 2(d), the continuous generation and disappearance of the dislocations result in the number of HCP atoms appears fluctuation the picture (e) corresponds to the point where the necking appears. In Fig.1(e), the necking instability happens at the 1/2 above the twin boundary when the nanowire deforms to 21%. The necking happens at the same position with specimen I when the nanowire deforms to 22% in Fig.2(e). Combining Fig.4(d) and Fig.5, we can observe that the larger the hole, the easier the necking appears and the easier the nanowires break.

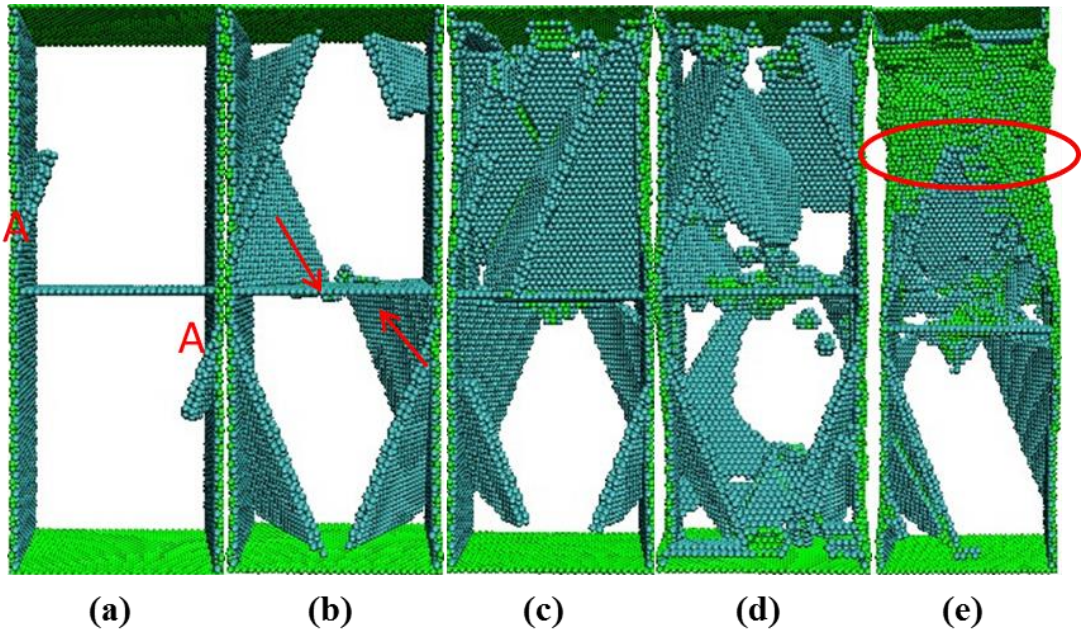

Fig.1 Tensile yielding of specimen I at 10 K. (a) The generation of the initial dislocation specimen I before yield point. (b) Atomic structure of the deformed sample at $\varepsilon = 4.5\%$. (c) Atomic structure of the deformed sample at $\varepsilon = 6.2\%$. (d) Atomic structure of the deformed sample at $\varepsilon = 10.0\%$. (e) Atomic structure of the deformed sample at $\varepsilon = 21.1\%$.

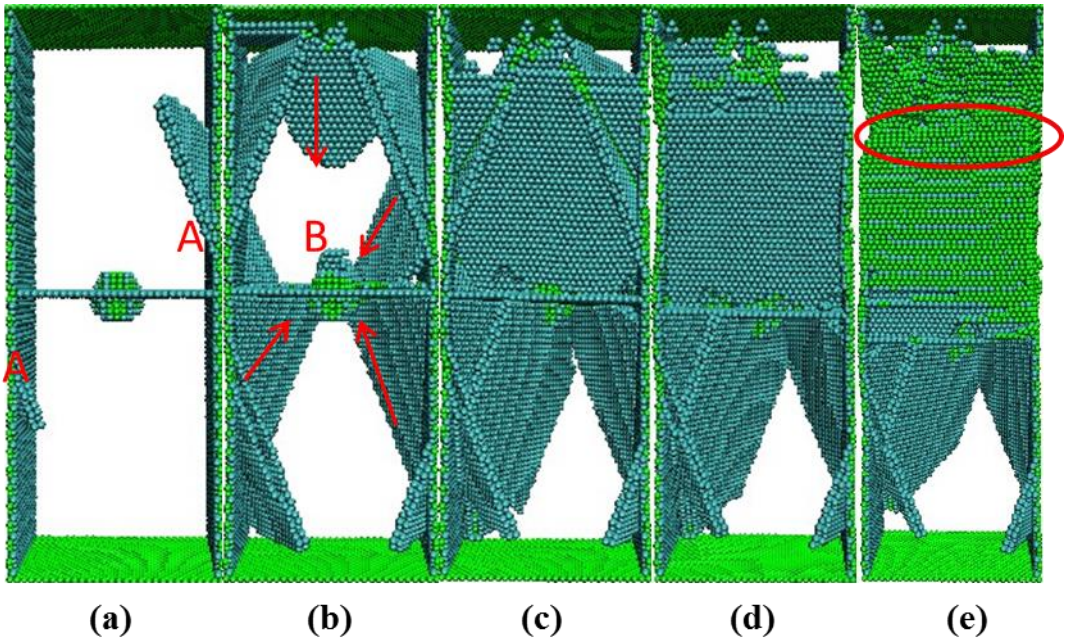

Fig.2 Tensile yielding of specimen III at 10 K. (a) The generation of the initial dislocation specimen III before yield point. (b) Atomic structure of the deformed sample at $\varepsilon = 4.6\%$. (c) Atomic structure of the deformed sample at $\varepsilon = 6.2\%$. (d) Atomic structure of the deformed sample at $\varepsilon = 10.0\%$. (e) Atomic structure of the deformed sample at $\varepsilon = 22.0\%$.